Author Manuscript

Author Manuscript

Author Manuscript

Author Manuscript

HHS Public Access

Author manuscript

Phys Med Biol. Author manuscript; available in PMC 2023 December 11.

Published in final edited form as:

Phys Med Biol. ; 67(21): . doi:10.1088/1361-6560/ac994f.

Assessment of bubble activity generated by histotripsy combined with echogenic liposomes

Aarushi Bhargava[1], **Shaoling Huang**[2], **David D. McPherson**[2], **Kenneth B. Bader**[1,*]

[1]Department of Radiology, University of Chicago, Chicago, 60637, USA.

[2]Department of Internal Medicine, Division of Cardiovascular Medicine, University of Texas Health Science Center-Houston, Houston, USA.

Abstract

Objective: Histotripsy is a form of focused ultrasound therapy that uses the mechanical activity of bubbles to ablate tissue. While histotripsy alone degrades the cellular content of tissue, recent studies have demonstrated it effectively disrupts the extracellular structure of pathologic conditions such as venous thrombosis when combined with a thrombolytic drug. Rather than relying on standard administration methods, associating thrombolytic drugs with an ultrasound-triggered echogenic liposome vesicle will enable targeted, systemic drug delivery. To date, histotripsy has primarily relied on nano-nuclei inherent to the medium for bubble cloud generation, and microbubbles associated with echogenic liposomes may alter the histotripsy bubble dynamics. The objective of this work was to investigate the interaction of histotripsy pulse with echogenic liposomes.

Approach: Bubble clouds were generated using a focused source in an *in vitro* vessel model. Acoustic emissions from the bubble oscillations were passively acquired to assess the mechanical activity of the bubble cloud. High frame rate, pulse inversion imaging was used to track the change in echogenicity of the liposomes following histotripsy exposure.

Main results: For peak negative pressures less than 20 MPa, acoustic emissions indicative of stable and inertial bubble activity were observed. Additional observations with high frame rate ultrasound imaging indicated fluid streaming around the focal region within the liposomal solutions at low and moderate pressures. As the peak negative pressure of the histotripsy excitation increased, harmonics of the excitation were observed in OFP t-ELIP solutions and plasma alone.

Significance: These observations suggest that a complex interaction between histotripsy pulses and echogenic liposomes which may be exploited for combination treatment approaches.

Keywords

Histotripsy; exogenous nuclei; echogenic liposomes; bubble dynamics; focused ultrasound

[*]Kenneth B. Bader: baderk@uchicago.edu.

Author Manuscript Author Manuscript Author Manuscript Author Manuscript

1. Introduction

Ablation is among the primary tools available to physicians to render tissue biologically inert. Histotripsy is a focused ultrasound therapy that generates bubble clouds spontaneously in tissue to achieve ablation (Bader *et al* 2019b). Several pathological conditions are under investigation as potential targets for histotripsy, including deep venous thrombosis (Xu *et al* 2021). For heterogenous pathologies, there is impetus to combine histotripsy with a therapeutic drug to improve therapeutic outcomes. Recent studies indicate combining histotripsy with a standard-of-care thrombolytic drug have synergistic effects that improve the treatment outcomes for venous thrombosis relative to either approach individually (Bader *et al* 2016b, Bollen *et al* 2020, Hendley *et al* 2021). Encapsulation of therapeutic drugs in a lipid vesicle could facilitate systemic, targeted delivery to increase treatment efficacy, reduce systemic toxicity, and reduce procedural complexity. Echogenic liposomes represent a moiety that enables targeting of therapeutics delivered via ultrasound activation of microbubble associated with the vesicle (Alkan-Onyuksel *et al* 1996). Histotripsy pulses have been primarily generated bubble clouds spontaneously. A suspension of echogenic liposomes represents a bubbly liquid, which may alter the resultant interaction between the histotripsy pulses and tissue (Wijngaarden 2007). A deeper understanding is thus needed to understand how echogenic liposomes will alter the histotripsy bubble dynamics.

In this study, the interaction between histotripsy pulses and echogenic liposomes will be examined. Bubble activity generated by histotripsy pulses in solutions with or without echogenic liposomes will be assessed using two imaging methods. First, passive cavitation imaging will be used to map the strength and extent of acoustic emissions generated by bubble oscillations. High frame rate, pulse inversion imaging will be used to assess the change in liposome echogenicity following histotripsy exposure.

2. Methods

2.1. Preparation of human fresh-frozen plasma

Eight units of human type-O fresh-frozen plasma were procured from a blood bank (Vitalant, Chicago, IL, USA), pooled, and aliquoted to 50 mL volumes. The aliquots were stored at −80 °C prior to use. For each experiment, one aliquot was equilibrated to atmospheric pressure at 37 °C over the course of 2 hours.

2.2. Preparation of OFP t-ELIP

Echogenic liposomes loaded with rt-PA and associated with octafluoropropane microbubbles (OFP t-ELIP) were prepared at the University of Texas Health Sciences Center (Houston, TX, USA) following an established protocol (Huang *et al* 2001). Briefly, 5 mg of lipids (1, 2-distearoyl-sn-glycero-3-phosphocholine (DSPC), 1,2-Dioleoyl-sn-glycero-3-phosphocholine (DOPC), 1,2-dipalmitoyl-sn-glycero-3-phosphoglycerol, (DPPG) and cholesterol) with a molar ratio of 46:23:23:8 were mixed in chloroform. Cholesterol and chloroform were obtained from Sigma Aldrich, Inc. (St Louis, MO, USA), while DSPC, DOPC, and DPPG were obtained from Avanti Polar Lipids, Inc. (Alabaster, AL, USA). The organic solvent was removed by evaporation under argon at 50 °C with constant rotation

Author Manuscript Author Manuscript Author Manuscript Author Manuscript

until a thin film of lipids formed on the vial wall. The resulting lipid film was then placed under vacuum overnight. The dried lipid film was rehydrated with 200 μL of rt-PA (1 mg/mL), 50 μL of double-distilled water, and 250 μL of 0.64 M Mannitol (Sigma Aldrich, Inc., St Louis, MO, USA) per mg of lipid. The liposomes were then centrifuged at 13,200 rpm for 20 min at 25 °C (Model 5415D, Eppendorf, Hauppauge, NY, USA) to separate the free rt-PA from lipid-associated rt-PA. The resultant liposomal pellet was resuspended in 400 μL of 0.32 M Mannitol, and stored in 2 mL glass vials at −70 °C for 2 hours with 4 mg lipid per vial. The samples were lyophilized at −56 °C for 48 hours, and then stored in 2 mL glass vials overnight at 4 °C. The headspace was evacuated from vials, and reloaded with 2 mL (1 atm partial pressure) of octafluoropropane.

Vials of OFP t-ELIP were shipped to the University of Chicago on dry ice and stored at 4 °C prior to use. Before reconstitution, each vial was evacuated with a laboratory wall vacuum (~ 10 mmHg) for 5 min. The vial was then charged with 2 mL (1 atm partial pressure) of OFP gas through the septum using a 22-gauge needle. The vial was equilibrized for 3 hours, and 0.4 mL of deionized (>18 MOhm-cm resistivity), and air saturated (100 ± 2%) water was then added through a septum. The mixture was gently agitated to form the liposome structure. The reconstituted OFP t-ELIP was diluted in human fresh frozen plasma within a minute to obtain lipid (rt-PA) concentrations of 11.3 μg/mL (0.27 μg/mL), 56.4 μg/mL (1.34 μg/mL), or 112.8 μg/mL (2.68 μg/mL). The highest rt-PA concentration corresponds to that administered for pharmacomechanical treatment of deep vein thrombosis (Hilleman and Razavi 2008). Most studies were conducted at a lipid (rt-PA) dose of 11.3 μg/mL (0.27 μg/mL) to minimize acoustic shadowing.

2.3. Histotripsy insonation

An eight-element focused transducer with elliptical geometry (9 cm major axis and 7 cm minor axis), and 6 cm focal length was used to generate histotripsy pulses (Maxwell et al 2021). The fundamental operating frequency of the transducer was 1.5 MHz, which produces a linear acoustic field with −6 dB dimensions of 4.9 mm x 0.9 mm x 1.1 mm along the axial, major, and minor axes, respectively (Hendley et al 2021). Histotripsy pulses of 10-cycle duration (6.66 μs) and peak negative pressure 0 (control) to 32 MPa were applied at a rate of ~ 0.1 Hz. A custom-designed class D amplifier and matching network were used to excite all the elements of the transducer in parallel (Maxwell et al 2017). For assessment of bubble activity, an L11–5v imaging array (Verasonics, Inc., Kirkland, WA, USA) controlled by a research ultrasound system (Vantage 128, Verasonics, Inc., Kirkland, WA, USA) was placed in a coaxial opening of the focused transducer.

2.4. Experimental setup

A schematic of the *in vitro* model of femoral vein is shown in figure 1. A 36 × 36 × 30 cm acrylic tank was filled with degassed (20 ± 5% dissolved oxygen), filtered (0.2 μm), reverse osmosis water heated to 37.3 ± 0.5°C. The degassing, filtration, and temperature of the water were continuously maintained throughout the experiments using a custom-built recirculation and temperature controller circuit (Bollen et al 2020). The tank walls were lined with acoustic absorbing sheets (Precision Acoustics, Dorcester, Dorcet, UK) to mitigate reflections of ultrasound waves from the tank walls.

Author Manuscript Author Manuscript Author Manuscript Author Manuscript

Plasma with or without liposomes was infused into a channel of latex tubing with 1.6 cm outer diameter and 0.16 cm thickness (McMaster-Carr, Elmhurtst, IL, USA). The diameter and acoustomechanical properties of the vessel model are similar to the common femoral vein (Hertzberg et al 1997). A syringe pump (EW-74900–20, Cole-Parmer, Vernon Hills, IL, USA) was employed in withdraw mode to perfuse the vessel model with plasma alone or plasma and liposomes. A three-axis motorized positioner (BiSlide, Velmex Inc., Bloomfield, NY, USA) was used to align the focal zone of the histotripsy source within the vessel model under ultrasound image guidance.

2.5. Experimental procedure

The vessel model was perfused with a fresh bolus of plasma alone or plasma and OFP t-ELIP. After flow had ceased (i.e. the perfusate was static), a single histotripsy pulse of 10 cycle duration (6.66 μs) and peak negative pressure ranging from 0 to 32 MPa was applied within the vessel model. The next pulse was applied after acquiring the imaging data and infusing a fresh bolus of perfusate into the vessel model. The time between pulses was approximately 11 s, and hence the pulse repetition frequency was ~ 0.1 Hz. For each experimental arm, a total of 50 pulses were examined over the course of three separate aliquots of OFP t-ELIP. With each aliquot, data was collected within 10 min to minimize dissolution of OFP t-ELIP (Radhakrishnan et al 2012). In total, data from 1,400 histotripsy pulses were analyzed.

2.6. Image acquisition and analysis

An L11–5v imaging array coaxial to the focused source was used to detect bubble activity, figure 1. Acoustic emissions generated during the pulse were passively detected with the array over a 60 μs duration starting 5 μs prior to insonation, figure 2. Emissions were processed offline with the robust Capon beamformer to form passive cavitation images (Coviello et al 2015). Each pixel of the passive cavitation image is proportional to the intensity of acoustic emissions at that location, and therefore strength of bubble oscillations (Haworth et al 2017). For each data set, the mean passive cavitation image pixel value within the lumen was tabulated. A piecewise linear function was fit using least-squares error criterion to the tabulated maximum emission levels as a function of the peak negative pressure of the histotripsy pulse. The peak negative pressure threshold required to initiate bubble activity was defined as the inflection point in the piecewise linear fit (Radhakrishnan et al 2013).

A plane wave, pulse inversion sequence was used to assess changes in OFP t-ELIP echogenicity prior to and following histotripsy exposure (Shen et al 2005). Pulse inversion imaging data was collected at a 2.5 kHz rate over a 26 ms duration to track changes in bubble grayscale intensity immediately following histotripsy exposure, figure 2. To avoid constructive interference between the imaging and therapy pulses, the first frame was acquired 400 μs after the histotripsy exposure. The average grayscale intensity of pixels within the vessel model was tracked over time. The reduction in the average grayscale intensity following histotripsy exposure was used to indicate the degree of liposome disruption, figure 3(b). The average grayscale intensity within the vessel model I was fit to a power law function of the form:

Author Manuscript Author Manuscript Author Manuscript Author Manuscript

$$I(t) = a*t^b + c \quad (1)$$

where a, b, and, c are fitting parameters, and t is time, figure 3(a). The initial rate of change in grayscale intensity was calculated as the time differential of the power law fit, figure 3(b). For all experimental arms, the grayscale intensity changed monotonically between 2 and 26 ms. Hence, the rate of change in pixel intensity was evaluated at 2 ms.

2.7. Statistical analysis

To compare statistical differences in acoustic emission levels and time-dependent grayscale behavior between experimental arms, a one-way ANOVA test along with Turkey's honest significant criterion was performed. Pearson's correlation coefficients were calculated to assess the dependence of these parameters on the histotripsy pulse peak negative pressure. A p-value of 0.05 was chosen for all tests. All statistical analysis was performed in MATLAB 2021b (MathWorks, Natick, MA, USA).

3. Results

3.1. Strength of bubble activity initiated by the histotripsy pulse

For plasma alone, no detectable level of bubble activity was noted for peak negative pressures less than ~ 23.3 MPa (figure 4, top row). For OFP t-ELIP solutions, low but detectable bubble activity was noted for all histotripsy pulses pressures explored in this study. For all exposure conditions, the peak emission levels were contained with the vessel model, consistent with prior studies (Hendley et al 2022).

The mean passive cavitation image pixel values within the lumen, a marker for the strength of bubble activity, are shown in figure 5 (N = 50 for each arm). For histotripsy pulse peak negative pressures less than 32 MPa, the emission levels generated from OFP t-ELIP solutions were increased by at least an order of magnitude relative to plasma alone, figure 4 and 5. For peak negative pressures of 32 MPa, the intensity of OFP t-ELIP emissions was increased relative to plasma alone by a factor of ~ 5.7. These data were fit to a piecewise linear function, and the inflection point defined the threshold peak negative pressure required to initiate bubble activity (Radhakrishnan et al 2013). For plasma alone, the inflection point was observed at 23.3 ± 0.02 MPa, corresponding to a passive cavitation image pixel value of 0.0014 ± 0.0003 V^2 (R^2 = 0.99 for the piecewise linear fit). For OFP t-ELIP solution, two inflection points were found to provide the best fit (R^2 = 0.95) at 5.7 ± 0.06 MPa (passive cavitation image pixel value of 0.001 ± 0.0005 V^2) and 19.2 ± 0.07 MPa (passive cavitation image pixel value of 0.03 ± 0.002 V^2).

3.2. Mode of generated bubble activity

The spectrum of acoustic emissions can be used as a means to characterize the type of bubble activity (Haworth et al 2017). Figure 6 displays the spectrum corresponding to the maximum passive cavitation pixel value for histotripsy pulse peak negative pressures of 4, 16, and 32 MPa. These pressures correspond to bubble activity generated by OFP t-ELIP below the first inflection point (black arrow, figure 5), between the two inflection points

Author Manuscript Author Manuscript Author Manuscript Author Manuscript

(black and red arrow, figure 5), and above the second inflection point (red arrow, figure 5), respectively. Multiple harmonics of the fundamental insonation frequency (1.5 MHz) were observed at the lowest pressure investigated for OFP t-ELIP solutions (4 MPa), indicative of stable bubble activity. In contrast, only the first harmonic was observed for plasma alone solution. Inharmonic emissions (i.e. frequencies between 4.5 and 10.5 MHz excluding 0.8 MHz bands around harmonic, subharmonic, and ultraharmonic emissions of the fundamental driving frequency of the histotripsy pulse) representative of inertial bubble activity were increased by 36% for OFP t-ELIP solutions relative to plasma alone for histotripsy pulse peak negative pressures of 4 MPa (Bader et al 2015).

For peak negative pressures of 16 MPa, harmonic emissions were consistently observed in plasma alone solutions. In contrast, harmonic emissions were not observed in OFP t-ELIP solutions at this excitation pressure. The precise reason for the lack of harmonic emissions is unknown, but is consistent with pressure waves emitted during inertial bubble activity (Bader et al 2015). Hence, inertial bubble activity may be the dominant oscillatory mode of OFP t-ELIP over this range of histotripsy pulse pressures. For peak negative pressures of 32 MPa, harmonics of the fundamental frequency of the histotripsy pulse were observed in emission spectra for solutions with and without OFP t-ELIP. The intensity of emissions was increased by 7 dB at 32 MPa in liposome solution relative to plasma alone, figure 6. Interestingly, the fourth (nominally 6 MHz) and fifth (nominally 7.5 MHz) harmonics were shifted by ~ 38 kHz and ~ 50 kHz respectively in the presence of OFP t-ELIP relative to plasma alone, figure 6(c). The observed frequency shift may be associated with movement of liposomes following histotripsy exposure (Pouliopoulos et al 2020).

3.3. Extent of bubble activity

The azimuthal extent of acoustic emissions at the histotripsy focus (60 mm depth along the range dimension) was also tabulated for all experimental arms. The extent was based on the azimuthal distance over which the intensity of acoustic emissions exceeded those measured at each respective inflection point (see figure 7 insert). For plasma alone, the azimuthal extent corresponded to acoustic emission levels that exceeded 0.07 V^2 (green arrow, figure 5). For OFP t-ELIP solutions, widths corresponding to emission levels that exceeded 0.06 V^2 (black arrow, figure 5) and 0.57 V^2 (red arrow, figure 5). The extent of emissions was not tabulated along the range dimension due to limitations in the point spread function for passive imaging along this dimension (Haworth et al 2017).

The azimuthal extent of bubble activity initially increased rapidly as the peak negative pressure exceeded each respective inflection point, figure 7. The extent of OFP t-ELIP emissions based on the first inflection point (passive cavitation image pixel value 0.06 V^2) was increased relative to plasma for all peak negative pressures. For peak negative pressures in excess of 20 MPa, the extent of bubble activity for OFP t-ELIP for both modes of bubble activity (i.e. emissions at either the first or second inflection point, figure 5) was increased relative to plasma. For a given peak negative pressure, the emission extent based on the second inflection point for OFP t-ELIP (passive cavitation image pixel value 0.57 V^2)was reduced relative to the extent calculated using the first inflection point.

Author Manuscript Author Manuscript Author Manuscript Author Manuscript

3.4. Change in grayscale value following histotripsy exposure

In the absence of liposomes, no change in the average pixel intensity was observed relative to baseline with high frame rate, pulse inversion imaging for peak negative pressures less than ~ 23 MPa, figure 8. Beyond this pressure level, the grayscale value increased by a factor of two relative to baseline just after insonation due to bubble cloud formation, figure 8(e) and Movie S1. The pixel intensity within the vessel model was restored to its nominal value within 3.9 ± 1.3 ms, consistent with prior observations for passive dissolution of histotripsy bubble clouds generated without exogenous nuclei (Bader et al 2019a).

The time-dependent echogenicity was more complex for OFP t-ELIP solutions. For histotripsy pulse peak negative pressures less than 5.7 MPa (lower inflection point, figure 6), the grayscale intensity was initially reduced and then increase over the course of 25 ms to within ~ 60% of its baseline value (supplemental Movies S2 - S4). As the histotripsy pulse pressure increased, the observed change in grayscale intensity over time transitioned. For histotripsy pulse peak negative pressures of 32 MPa, the grayscale intensity decreased in monotonically figure 8(f), qualitatively similar to that observed for plasma alone, figure 8(e).

Metrics to quantify the change in the average grayscale intensity within the vessel model over time (minimum echogenicity and change in echogenicity during 25 ms of image acquisition, see figure 3) are shown in figure 9. The fitting parameters based on a least-squared fit of equation 1 to the change in the mean grayscale intensity within the lumen over time are listed in supplementary tables 1 and 2. For plasma alone solution, the minimum pixel value following histotripsy excitation remained constant and approximately equal to that prior to histotripsy pulse exposure. In contrast, minimum grayscale values decreased as the histotripsy pulse peak negative pressure increased for OFP t-ELIP solutions ($\rho = -0.8$; $p < 0.05$), figure 9(a).

Using a power law fit of the change in grayscale intensity over time via Eq. (1), the rate of change in echogenicity between 0 and 26 ms was also tabulated (see figure 3). For plasma alone solutions, there was no observed change in grayscale intensity for peak negative pressures less than ~ 23 MPa, figure 9(b). For peak negative pressures in excess of 23.3 MPa, a strong reduction in signal was observed due to passive dissolution of the spontaneously generated bubble cloud. For OFP t-ELIP solutions, the grayscale intensity initially increased following excitation for peak negative pressures less than 5.7 MPa (e.g. positive rate of echogenicity change). At intermediate driving levels (peak negative pressures between 5.7 and 20 MPa), no changes in the grayscale intensity were noted between 0 and 26 ms. At the highest driving levels (peak negative pressures greater than 20 MPa), the grayscale decreased over time, similar to that for plasma alone solutions but at a significantly reduced rate ($p < 0.05$).

3.5. The effect of OFP t-ELIP concentration on bubble dynamics

The concentration of liposomes reflects the total potential dose of therapeutic that can be delivered, and also the total number of microbubbles in suspension. The strength of acoustic emissions was found to vary significantly ($p < 0.05$) with OFP t-ELIP concentration for the insonation peak negative pressure of 8 MPa, but not at other pressure amplitudes,

Author Manuscript Author Manuscript Author Manuscript Author Manuscript

figure 10(a). Significant variability ($p < 0.05$) was also observed in the azimuthal extent of bubble activity with concentration for peak negative pressure of 8 MPa, but not at other pressure levels, figure 10(b). Observations with high frame-rate imaging indicated liposome concentration affected the time-dependent echogenicity of OFP t-ELIP, though no definitive trends were observed, figures 10(c) and 10(d).

4. Discussion

4.1. Threshold peak negative pressure for OFP t-ELIP activation by histotripsy pulses

Two thresholds that demarcated a change in the observed bubble dynamics were observed here for OFP t-ELIP solutions, figures 4 and 5. Prior studies have indicated that different modes of bubble activity are activated based on the driving pressure (Gruber et al 2014). These transitions have been classified from one form of stable bubble oscillations to another (e.g. harmonic to subharmonic oscillations) or from stable oscillations to inertial oscillations (Flynn 1964). A transition was observed here at 5.7 MPa peak negative pressure at which OFP t-ELIP exhibited purely inertial bubble activity, consistent to a separate study assessing histotripsy excitation of microbubbles (5.7 MPa vs. 4.29 MPa). Interestingly, the prior study indicated minimal tissue ablation at this driving level (Edsall et al 2021), suggesting histotripsy relies on bubble activity beyond standard inertial bubble activity.

Indeed, a secondary threshold observed here indicated an additional transition as the peak negative pressure approaches that typical for histotripsy (i.e. > 20 MPa). Hence, inertial bubble activity may not be the most effective descriptor for histotripsy. Prior studies with high-speed videography indicate histotripsy bubbles remain expanded for extended periods (Maxwell et al 2011), potentially due to extensive gas influx (Bader and Bollen 2018). Further these bubbles scatter the incident shock wave geometrically. Interestingly, a difference was noted between the second threshold identified for OFP t-ELIP solutions (~ 19.2 MPa) and the threshold observed for plasma alone (~ 23.3 MPa). The difference in these threshold peak negative pressures may reflect that OFP t-ELIP is large enough to scatter the incident histotripsy pulse geometrically. In contrast, increased pressure levels beyond shock wave formation may be necessary for spontaneous nucleation and bubble growth large enough for geometric scattering. Further studies are required to confirm this hypothesis.

4.2. Type of bubble activity initiate by histotripsy pulses

The type of bubble activity initiated will vary based on several factors, including the peak negative pressure of the histotripsy pulse (Holland and Apfel 1989). For peak negative pressures less than 5.7 MPa, there were no discernable bubble activity detected either via passive or active imaging. In contrast, OFP t-ELIP solutions displayed harmonics of the fundamental frequency of the histotripsy pulse (1.5 MHz) and inharmonic emissions. This spectrum of emissions is consistent with a mixture of stable and inertial bubble activity (Gruber et al 2014). Over this same range of histotripsy pulse pressures, the grayscale intensity of OFP t-ELIP was found to initially be reduced, but then restored to withing 60% of its baseline value within 25 ms of the excitation. There are many potential reasons for this observed phenomena. Acoustic streaming from the incident histotripsy pulse may

Author Manuscript Author Manuscript Author Manuscript Author Manuscript

cause local mixing (Nyborg 1953). Microstreaming from stable bubble oscillations may also attract nearby intact liposomes (Collis et al 2010). Regardless, excitation conditions that do not destroy the entire population of liposomes (i.e. stable bubble oscillations and not totally inertial oscillations) appears to critical

For the intermediate peak negative pressure levels explored in this study (5.7 to 20 MPa), inertial oscillations associated with inharmonic emissions were the primary mode of bubble activity detected from OFP t-ELIP, figure 6. In contrast, harmonics of the fundamental frequency of the histotripsy were detected for plasma alone solutions. These harmonics may indicate fundamental scattering of the incident nonlinear pressure wave and not bubble activity (Haworth et al 2012, Thies and Oelze 2022). Indeed, there was no indication of changes in the grayscale intensity on the pulse inversion sequence to suggest bubble activity for plasma alone solutions. Minimal changes were observed in the grayscale intensity for OFP t-ELIP solutions, though the intensity was reduced to ~ 40% of the baseline value. These data suggest nearly instantaneous destruction of the liposomes that persist for the observation period (26 ms). Here, the perfusate was stagnant between the application of pulses. In the presence of vascular flow, it is likely an influx of OFP t-ELIP could cause the grayscale intensity to increase over time following the excitation. The degree of influx will have an influence on the resultant histotripsy bubble dynamics, which will be the subject of future studies.

Strong harmonic emissions were observed in both plasma alone and OFP t-ELIP solutions at peak negative pressures of ~ 20 and 23.3 MPa, respectively. The observed similarity in spectra for both solutions suggest a corresponding similarity in the type of bubble activity. There may be multiple reasons for this similarity. Nuclei inherent to the plasma are hypothesized to be nanoscale in size (Maxwell et al 2013). For peak negative pressures greater than 20 MPa, the histotripsy pulse is highly nonlinear and at the onset of shock wave formation (Maxwell et al 2021). Prior studies have demonstrated that histotripsy bubble dynamics are largely independent of the nucleus size for highly nonlinear excitations (Bader et al 2016b). Another possibility is that both types of nuclei generate bubbles large enough to induce geometric scattering of incident wave. The shocked histotripsy pulses have substantial harmonic content (Bader et al 2016a), with a spatial thickness shorter than either the quiescent microbubbles or bubble nucleated directly from the plasma solution.

Agreement in the mode of bubble activity for solutions with an without OFP t-ELIP was also observed in the pulse inversion imaging data. A monotonic decrease in the grayscale intensity was observed for all tested solutions at these driving levels (figures 8, and Movies S1 and S5). The grayscale intensity decreased more quickly for plasma compared to OFP t-ELIP solutions (176 grayscale/s vs. 44 grayscale/s). Perfluorocarbon gases such as octafluoropropane have a reduced solubility in plasma compared to air (Riess 2005, Spiess 2009), and these data indicate bubble clouds generated from OFP t-ELIP will dissolve more slowly than those generated spontaneously. Persistent bubble activity is known to alter the histotripsy ablation profile (Wang et al 2012), and advanced exposure schemes may be required to ensure effective clot fractionation in the presence of OFP t-ELIP.

Author Manuscript Author Manuscript Author Manuscript Author Manuscript

4.3. Clinical implications for use of histotripsy with OFP t-ELIP

Histotripsy alone is capable of cellular lysis, but is less effective at breaking down extracellular components that also contribute to pathologic malignancies (Vlaisavljevich et al 2013). Combining histotripsy with a targeted moiety will enable treatment of cellular and extracellular structures. Echogenic liposomes represent a potential moiety that can be administered systemically to reduce the treatment complexity and causticity associated with particular therapeutic drugs. The findings here indicate no change in the type of bubble activity generated from echogenic liposomes relative to bubbles generated spontaneously. Further, the intensity of acoustic emissions is increased by more than a factor of four for OFP t-ELIP arms relative to plasma alone (figure 5). A prior study indicated that the intensity of bubble cloud acoustic emissions correlated with the degree of tissue ablation (Bader et al 2018). The implications of this study thus indicate combining histotripsy with OFP t-ELIP will provide robust tissue degradation and treatment efficacy relative to histotripsy alone. However, further studies are required to confirm this conclusion. Additional studies are also required to determine the safety of this combination therapy prior to translation into the clinic.

4.4. Limitations

There are several aspects of this study that limit the generalizability of these findings. The perfusate was static, whereas vascular flow may alter distribution of liposomes following histotripsy exposure. The bubble dynamics were assessed based on application of a single histotripsy pulse, whereas up to thousands of pulses may be applied during clot treatment (Wang et al 2012). The *in vitro* nature of the study also precluded the assessment of off-target histotripsy ablation or systemic effects of therapeutic within the liposomes, which will be assessed in future studies *in vivo*. Here, acoustic methods were used to assess the bubble dynamics resulting from interaction between the histotripsy pulse and echogenic liposomes. High speed videography enables direct visual observation of the bubble dynamics and scattering of the excitation pulse (Maxwell et al 2011). Though videography is informative, it is not a viable option to assess bubble activity in opaque media (i.e. tissue). In addition to the histotripsy pulse, the pulse inversion sequence may also have contribute to changes in the bubble cloud grayscale intensity. Prior studies have noted vial-to-vial variability in the size distribution and acoustic attenuation for OFP t-ELIP (Shekhar et al 2017), which may contribute to the spread in data reported here for each arm. For passive imaging, correction factors such as array sensitivity, attenuation, and diffraction were not included (Gray et al 2018). Hence, the comparison of the intensity of acoustic emissions detected with passive cavitation imaging between arms should be considered relative and not absolute. Further, analysis of bubble cloud emissions with passive cavitation imaging was restricted along the azimuthal dimension due to limitations in the resolution along the range dimension (Haworth et al 2017). The objective of this study was to assess the influence of echogenic liposomes on histotripsy bubble dynamics. The precise nature of the relationship between this bubble activity and tissue disruption was not assessed, and will be the focus of future studies.

Author Manuscript Author Manuscript Author Manuscript Author Manuscript

5. Conclusions

The goal of this study was to examine the interaction between histotripsy pulses and echogenic liposomes. For pulse peak negative pressures typical of histotripsy (i.e. > 20 MPa), the type of bubble activity was similar between plasma alone and OFP t-ELIP solutions. The intensity of acoustic emissions was increased by at least a factor of four in OFP t-ELIP solutions relative to plasma alone at these pressure levels. In contrast, bubble activity representative of stable and inertial oscillations was observed at lower driving levels for OFP t-ELIP solutions (< 4 MPa peak negative pressure), but not plasma alone. Observations with high frame rate imaging also indicated a shift in the bubble dynamics for OFP t-ELIP solutions with the histotripsy pulse pressure. Overall, these findings suggest a complex interaction between the histotripsy pulse and echogenic liposomes which may provide an effective systemic treatment for several pathological conditions.

Supplementary Material

Refer to Web version on PubMed Central for supplementary material.

References

Alkan-Onyuksel H, Demos SM, Lanza GM, Vonesh MJ, Klegerman ME, Kane BJ, Kuszak J and McPherson DD 1996 Development of inherently echogenic liposomes as an ultrasonic contrast agent J. Pharm. Sci. 85 486–90 [PubMed: 8742939]

Bader KB and Bollen V 2018 The influence of gas diffusion on bubble persistence in shock-scattering histotripsy J. Acoust. Soc. Am 143 EL481–6 [PubMed: 29960422]

Bader KB, Crowe MJ, Raymond JL and Holland CK 2016a Effect of frequency-dependent attenuation on predicted histotripsy waveforms in tissue-mimicking phantoms Ultrasound Med. Biol. 42 1701–5

Bader KB, Gruber MJ and Holland CK 2015 Shaken and stirred: Mechanisms of ultrasound-enhanced thrombolysis Ultrasound Med. Biol. 41 187–96

Bader KB, Haworth KJ, Maxwell AD and Holland CK 2018 Post hoc analysis of passive cavitation imaging for classification of histotripsy-induced liquefaction in vitro IEEE Trans. Med. Imaging 37 106–15

Bader KB, Haworth KJ, Shekhar H, Maxwell AD, Peng T, McPherson DD and Holland CK 2016b Efficacy of histotripsy combined with rt-PA in vitro Phys. Med. Biol 61 5253–74 [PubMed: 27353199]

Bader KB, Hendley SA, Anthony GJ and Bollen V 2019a Observation and modulation of the dissolution of histotripsy-induced bubble clouds with high-frame rate plane wave imaging Phys. Med. Biol 64 115012

Bader KB, Vlaisavljevich E and Maxwell AD 2019b For whom the bubble grows: Physical principles of bubble nucleation and dynamics in histotripsy ultrasound therapy Ultrasound Med. Biol. 45 1056–1080

Bollen V, Hendley SA, Paul JD, Maxwell AD, Haworth KJ, Holland CK and Bader KB 2020 In Vitro Thrombolytic Efficacy of Single- and Five-Cycle Histotripsy Pulses and rt-PA Ultrasound Med. Biol. 46 336–349

Collis J, Manasseh R, Liovic P, Tho P, Ooi A, Petkovic-Duran K and Zhu Y 2010 Cavitation microstreaming and stress fields created by microbubbles Ultrasonics 50 273–9 [PubMed: 19896683]

Coviello C, Kozick R, Choi J, Gyöngy M, Jensen C, Smith PP and Coussios C-C 2015 Passive acoustic mapping utilizing optimal beamforming in ultrasound therapy monitoring J. Acoust. Soc. Am 137 2573–85 [PubMed: 25994690]

Author Manuscript Author Manuscript Author Manuscript Author Manuscript

Edsall C, Khan ZM, Mancia L, Hall S, Mustafa W, Johnsen E, Klibanov AL, Durmaz YY and Vlaisavljevich E 2021 Bubble cloud behavior and ablation capacity for histotripsy generated from intrinsic or artificial cavitation nuclei Ultrasound Med. Biol. 47 620–39

Flynn HG 1964 Physics of Acoustic Cavitation in liquids Physical Acoustics ed W P Mason (New York: Academic Press, Inc) pp 58–172

Gray MD, Lyka E and Coussios CC 2018 Diffraction Effects and Compensation in Passive Acoustic Mapping IEEE Trans. Ultrason. Ferroelectr. Freq. Control 65 258–68

Gruber MJ, Bader KB and Holland CK 2014 Cavitation thresholds of contrast agents in an in vitro human clot model exposed to 120-kHz ultrasound J. Acoust. Soc. Am 135 646–53 [PubMed: 25234874]

Haworth KJ, Bader KB, Rich KT, Holland CK and Mast TD 2017 Quantitative frequency-domain passive cavitation imaging IEEE Trans. Ultrason. Ferroelectr. Freq. Control 64 177–91

Haworth KJ, Mast TD, Radhakrishnan K, Burgess MT, Kopechek JA, Huang S-L, McPherson DD and Holland CK 2012 Passive imaging with pulsed ultrasound insonations J. Acoust. Soc. Am 132 544 [PubMed: 22779500]

Hendley SA, Bhargava A, Holland CK, Wool GD, Ahmed O, Paul JD and Bader KB 2022 (More than) doubling down: Effective fibrinolysis at a reduced rt-PA dose for catheter-directed thrombolysis combined with histotripsy PLoS One 17 e0261567

Hendley SA, Paul JD, Maxwell AD, Haworth KJ, Holland CK and Bader KB 2021 Clot Degradation Under the Action of Histotripsy Bubble Activity and a Lytic Drug IEEE Trans. Ultrason. Ferroelectr. Freq. Control 68 2942–52

Hertzberg BS, Kliewer MA, DeLong DM, Lalouche KJ, Paulson EK, Frederick MG, Carroll BA 1997 Sonographic assessment of lower limb vein diameters: implications for the diagnosis and characterization of deep venous thrombosis. Am Roentgen Ray Soc 168 1253–7

Hilleman DE and Razavi MK 2008 Clinical and Economic Evaluation of the Trellis-8 Infusion Catheter for Deep Vein Thrombosis J. Vasc. Interv. Radiol 19 377–83 [PubMed: 18295697]

Holland CK and Apfel RE 1989 Improved Theory for the Prediction of Microcavitation Thresholds IEEE Trans. Ultrason. Ferroelectr. Freq. Control 36 204–8

Huang S-L, Hamilton AJ, Nagaraj A, Tiukinhoy SD, Klegerman ME, McPherson DD and MacDonald RC 2001 Improving ultrasound reflectivity and stability of echogenic liposomal dispersions for use as targeted ultrasound contrast agents J. Pharm. Sci 90 1917–26 [PubMed: 11745750]

Maxwell AD, Cain CA, Hall TL, Fowlkes JB and Xu Z 2013 Probability of cavitation for single ultrasound pulses applied to tissues and tissue-mimicking materials Ultrasound Med. Biol. 39 449–65

Maxwell AD, Haworth KJ, Holland CK, Hendley SA, Kreider W and Bader KB 2022 Design and characterization of an ultrasound transducer for combined histotripsy-thrombolytic therapy IEEE Trans. Ultrason. Ferroelectr. Freq. Control 69 156–165

Maxwell AD, Wang T-Y, Cain CA, Fowlkes JB, Sapozhnikov OA, Bailey MR and Xu Z 2011 Cavitation clouds created by shock scattering from bubbles during histotripsy J. Acoust. Soc. Am 130 1888

Maxwell AD, Yuldashev PV, Kreider W, Khokhlova TD, Schade GR, Hall TL, Sapozhnikov OA, Bailey MR and Khokhlova VA 2017 A prototype therapy system for transcutaneous application of boiling histotripsy Ultrason. Ferroelectr. Freq. Control. IEEE Trans 64 1542–57

Nyborg WL 1953 Acoustic streaming due to attenuated plane waves J. Acoust. Soc. Am 25 68

Pouliopoulos AN, Smith CAB, Bezer JH, El Ghamrawy A, Sujarittam K, Bouldin CJ, Morse SV., Tang MX and Choi JJ2020 Doppler passive acoustic mapping IEEE Trans. Ultrason. Ferroelectr. Freq. Control 67 2692–703

Radhakrishnan K, Bader KB, Haworth KJ, Kopechek JA, Raymond JL, Huang SL, McPherson DD and Holland CK 2013 Relationship between cavitation and loss of echogenicity from ultrasound contrast agents Phys. Med. Biol 58 6541–63

Radhakrishnan K, Haworth KJ, Huang S-L, Klegerman ME, McPherson DD and Holland CK 2012 Stability of echogenic liposomes as a blood pool ultrasound contrast agent in a physiologic flow Phantom Ultrasound Med. Biol. 38 1970–81

Author Manuscript Author Manuscript Author Manuscript Author Manuscript

Riess JG 2005 Understanding the fundamentals of perfluorocarbons and perfluorocarbon emulsions relevant to in vivo oxygen delivery Artif. Cells. Blood Substit. Immobil. Biotechnol 33 47–63

Shekhar H, Bader KB, Huang S, Peng T, Huang S, McPherson DD and Holland CK 2017 In vitro thrombolytic efficacy of echogenic liposomes loaded with tissue plasminogen activator and octafluoropropane gas Phys. Med. Biol 62 517–38 [PubMed: 28002053]

Shen CC, Chou YH and Li PC 2005 Pulse inversion techniques in ultrasonic nonlinear imaging J. Med. Ultrasound 13 3–17

Spiess BD 2009 Perfluorocarbon emulsions as a promising technology: a review of tissue and vascular gas dynamics J. Appl. Physiol 106 1444–52 [PubMed: 19179651]

Thies M and Oelze ML 2022 Combined therapy planning, real-time monitoring, and low intensity focused ultrasound treatment using a diagnostic imaging array IEEE Trans. Med. Imaging 41 1410–9 [PubMed: 34986094]

Vlaisavljevich E, Kim Y, Owens G, Roberts W, Cain C and Xu Z 2013 Effects of tissue mechanical properties on susceptibility to histotripsy-induced tissue damage Phys. Med. Biol 59 253–70 [PubMed: 24351722]

Wang T-Y, Xu Z, Hall TL, Fowlkes JB and Cain CA 2012 An efficient treatment strategy for histotripsy by removing cavitation memory Ultrasound Med. Biol. 38 753–66

Wijngaarden L van2007 Shock waves in bubbly liquids Shock wave science and technology reference library (Berlin, Heidelberg: Springer Berlin Heidelberg) pp 3–33

Xu Z, Hall TL, Vlaisavljevich E and Lee FT 2021 Histotripsy: the first noninvasive, non-ionizing, non-thermal ablation technique based on ultrasound Int. J. Hyperth 38 561–75

Author Manuscript Author Manuscript Author Manuscript Author Manuscript

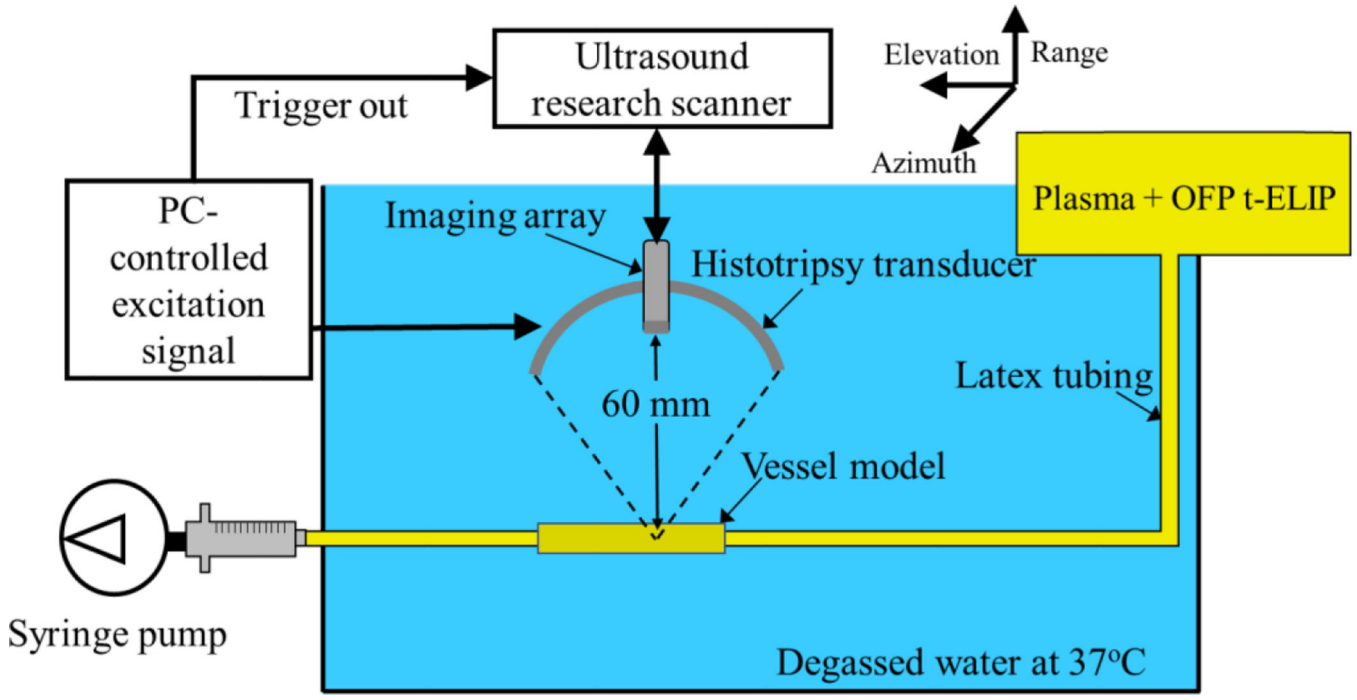

Figure 1.

Schematic of experimental setup. Plasma with or without echogenic liposomes (OFP-t-ELIP) was perfused through a vessel model. A focused source was used to apply a histotripsy pulse to the solution within the vessel model. A fresh bolus of solution was drawn into the vessel model after each insonation. An imaging array controlled by a research ultrasound system was used to collect data on bubble dynamics initiated by the histotripsy pulse. The dimensional axes are in reference to the imaging array.

Author Manuscript Author Manuscript Author Manuscript Author Manuscript

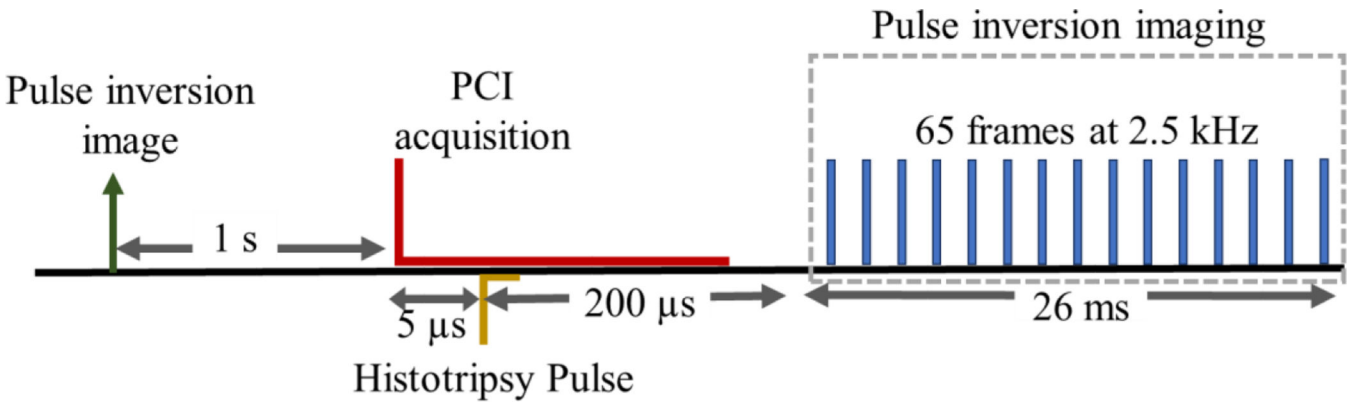

Figure 2.

Timing diagram for the acquisition of imaging data to assess histotripsy bubble activity. For each applied histotripsy pulses, passive cavitation imaging (PCI) was used to assess the strength and the spatial extent of acoustic emissions. A plane wave, pulse inversion sequence was used to assess changes in the echogenicity of liposome solutions over a 26 ms period at a 2.5 kHz frame rate following the insonation. To determine the baseline echogenicity, a plane wave, pulse inversion image was also acquired prior to application of the histotripsy pulse.

Author Manuscript Author Manuscript Author Manuscript Author Manuscript

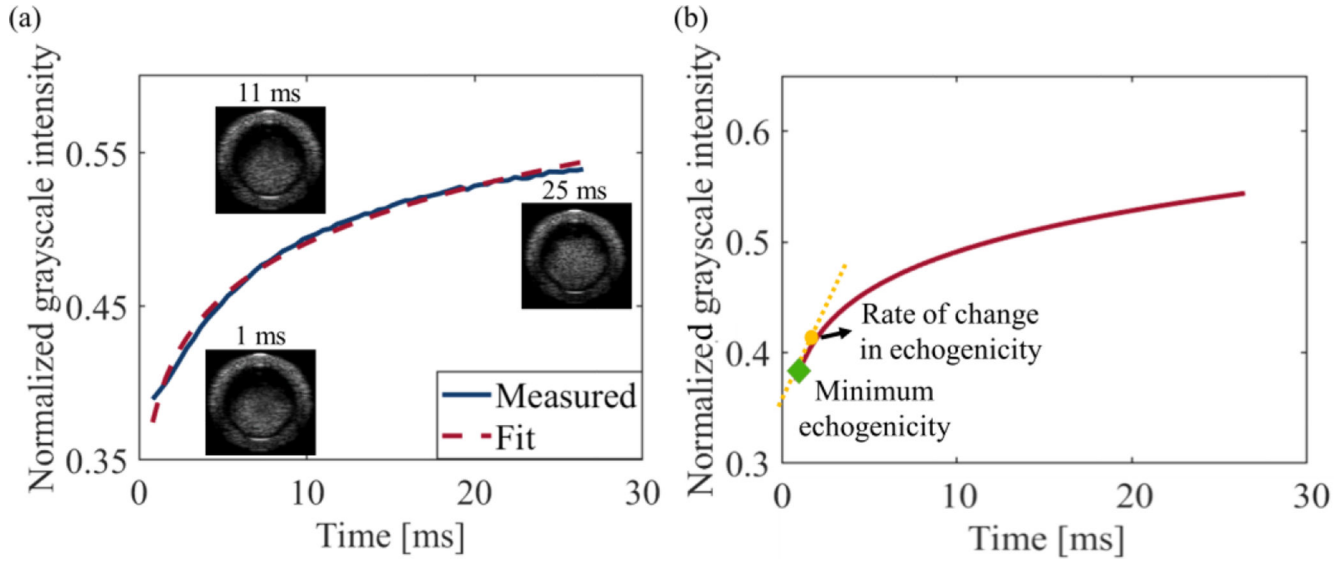

Figure 3.

(a) Representation of the variation in grayscale intensity within the vessel model following the histotripsy pulse exposure at 2 MPa. The data is approximated with a power law function (dashed line) via Eq. (1). (b) The minimum echogenicity (shown by green diamond) was defined as the minimum grayscale value observed following insonation. The rate of change of grayscale intensity was calculated as the time differential of the power law fit Eq. (1) at 2 ms (slope shown as yellow dotted line).

Author Manuscript Author Manuscript Author Manuscript Author Manuscript

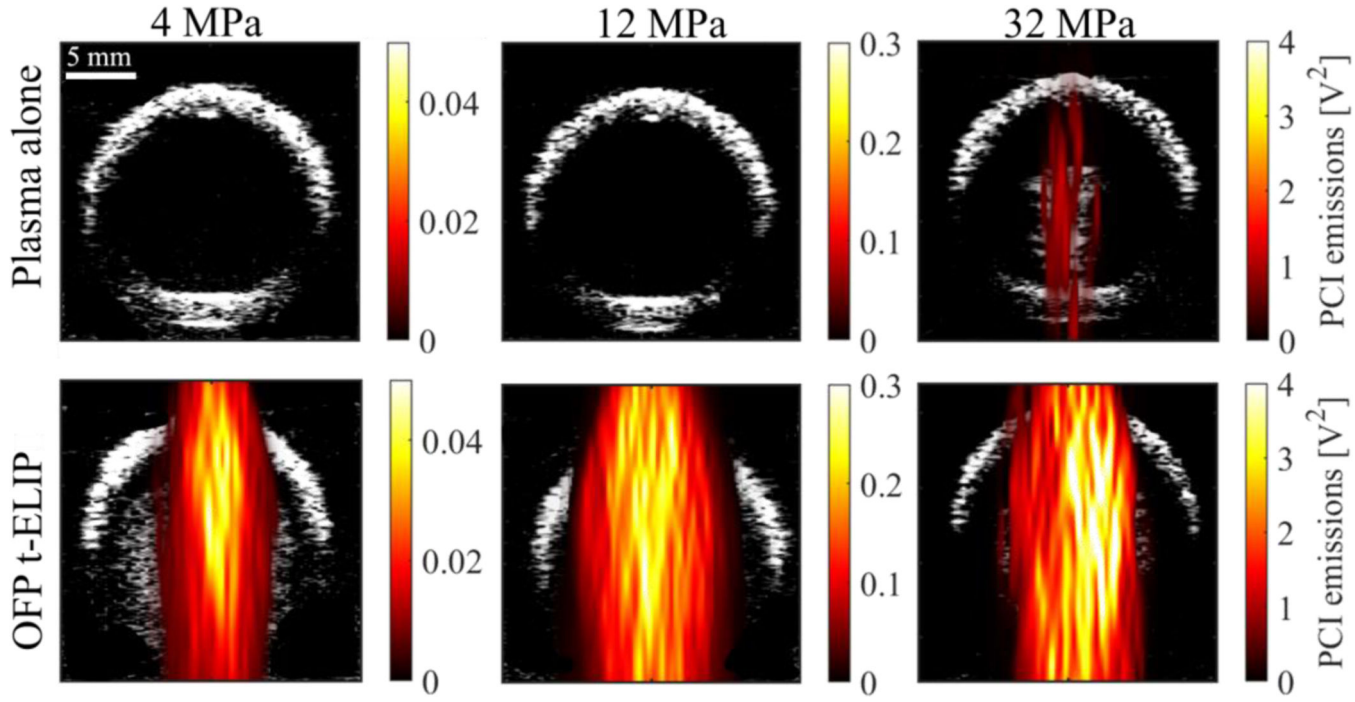

Figure 4.

Passive cavitation image (PCI) (hot color map) overlaid with pulse inversion image of vessel model. The top and bottom rows show passive cavitation images for solutions without and with OFP t-ELIP (11.3 μg/mL), respectively. The peak negative pressure of the histotripsy pulse is noted at the top of each column. Note that the range of reported emissions levels differ for each column.

Author Manuscript Author Manuscript Author Manuscript Author Manuscript

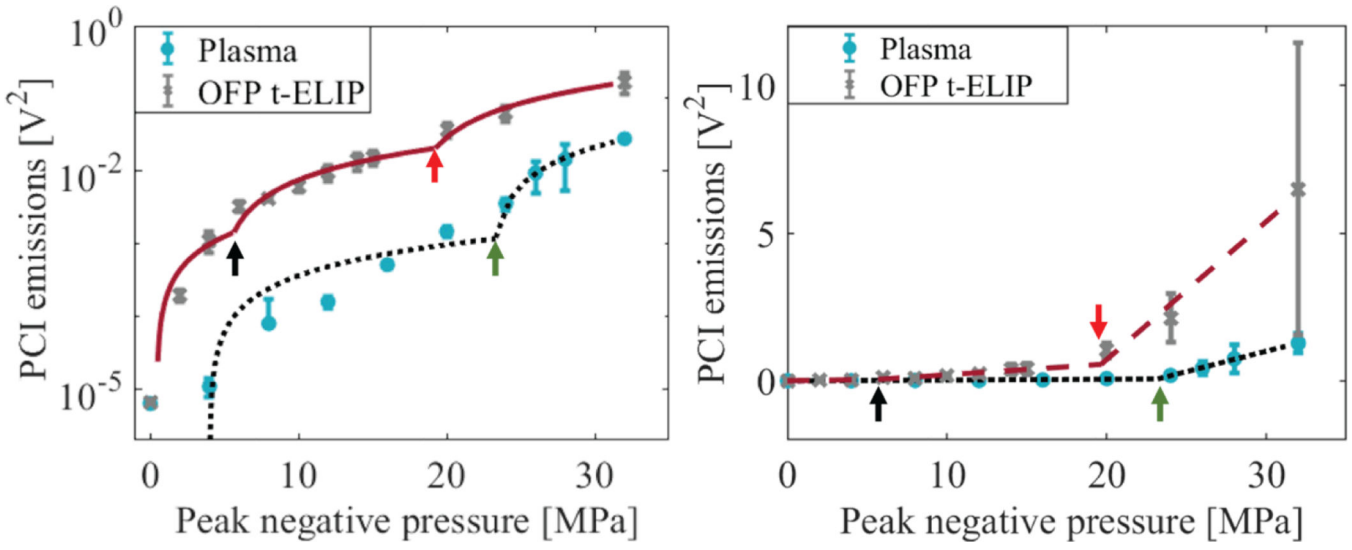

Figure 5.

Mean intensity of acoustic emissions detected within the lumen for solutions with and without OFP t-ELIP. The emissions levels are reported with log compression (left) and a linear scale (right). The solid (dashed) lines represent piece-wise linear fits between the emission intensity and the histotripsy pulse peak negative pressure for arms with (without) OFP t-ELIP. The black and red arrows denote the inflection points of the piece-wise linear fit for the OFP t-ELIP solution, and the green arrow represents the inflection point for the plasma alone solution. Each datapoint represents the mean of 50 datasets, and error bars the standard deviation.

Author Manuscript Author Manuscript Author Manuscript Author Manuscript

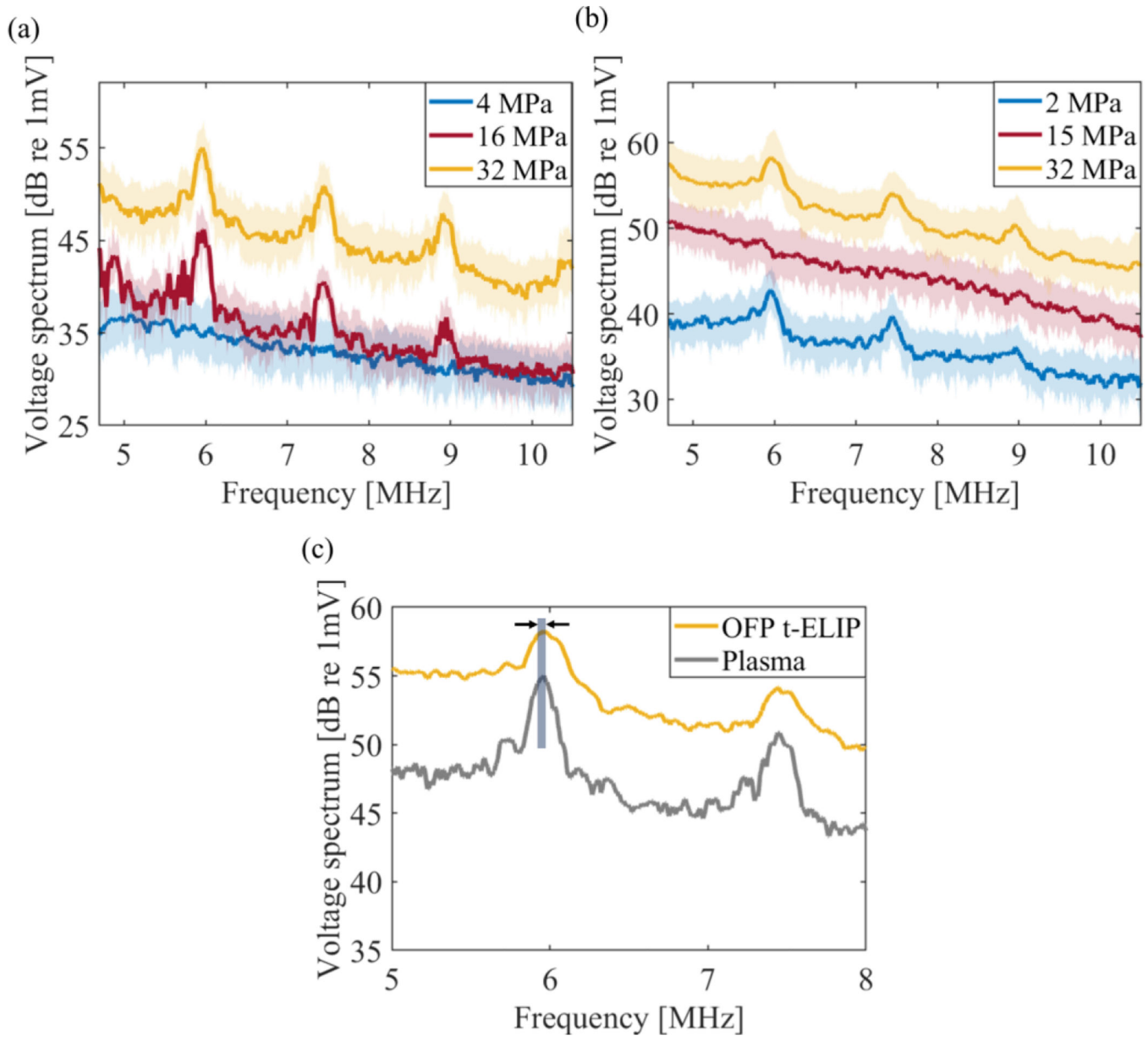

Figure 6.

Spectrum of signal corresponding to the maximum passive cavitation image pixel value (a) without and (b) with 11.3 μg/mL OFP t-ELIP, respectively. Solid lines are the mean of 50 data sets, with shading indicating the standard deviation. The peak negative pressure of the insonation pulse is included in the legend. (c) Spectra near the fourth and fifth harmonic of the histotripsy pulse fundamental frequency (1.5 MHz) at peak negative pressure of 32 MPa. for solutions with and without liposomes. The shaded box emphasizes the ~ 38 kHz frequency shift in the observed spectral peak for solutions with liposomes relative to plasma alone.

Author Manuscript Author Manuscript Author Manuscript Author Manuscript

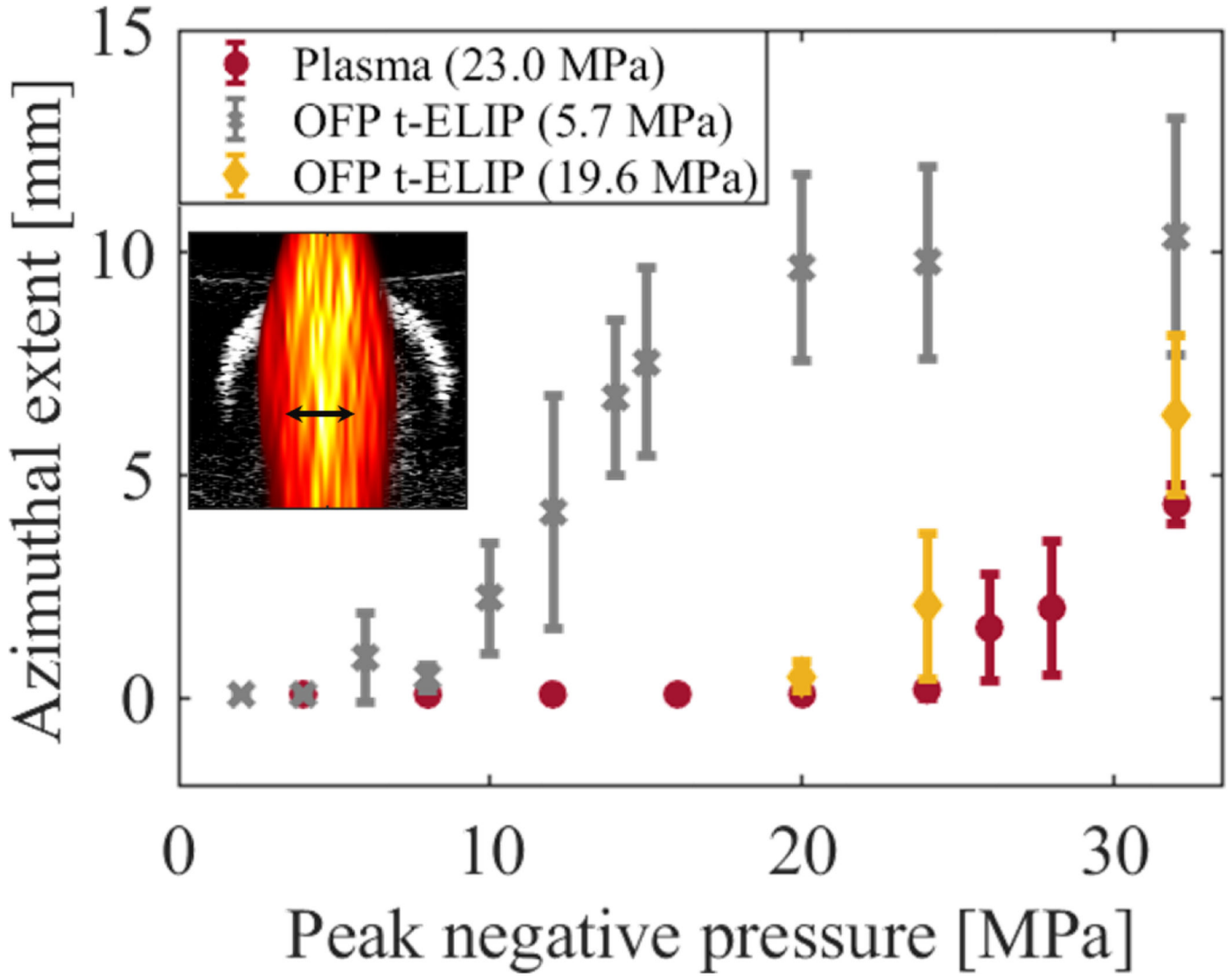

Figure 7.

The extent of the acoustic emission that exceed those observed at the onset of bubble activity (see figure 5). For OFP t-ELIP, inflection points were observed at 5.7 MPa and 19.2 MPa peak negative pressure of the histotripsy pulse. Only one inflection point was observed for plasma alone, corresponding to a histotripsy pulse peak negative pressure of 23.3.0 MPa. A total of 50 datasets were acquired for each pressure evaluated.

Author Manuscript Author Manuscript Author Manuscript Author Manuscript

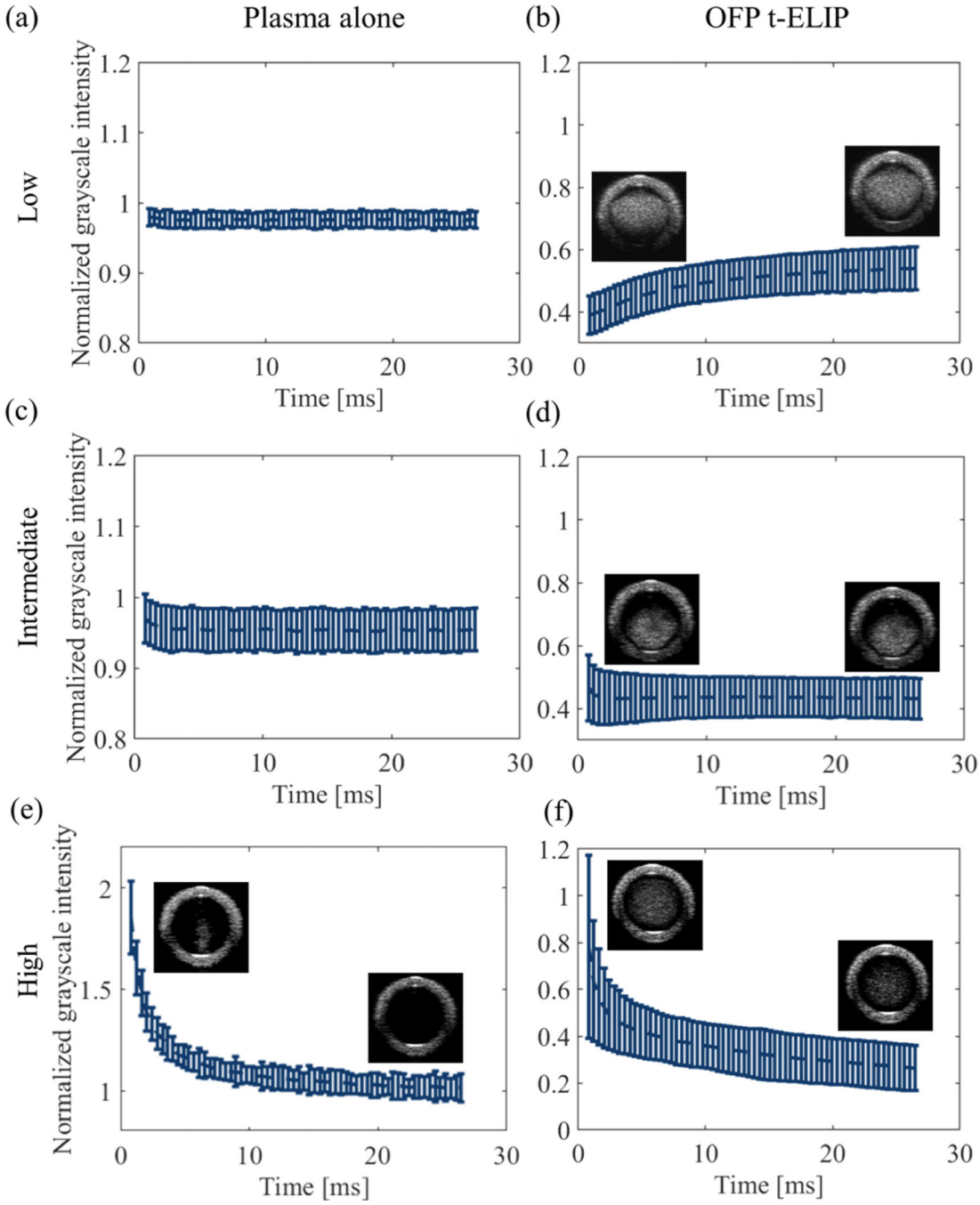

Figure 8.

Change in grayscale intensity within the vessel model observed with the high frame rate, pulse inversion imaging sequence at peak negative pressures of (a, b) ~ 4 MPa, (c, d) ~ 16 MPa, and (e, f) ~ 32 MPa for plasma alone solution (left column) and OFP t-ELIP solutions (11.3 μg/mL, right column). The grayscale intensity was normalized with respect to the vessel model grayscale intensity prior to application of the histotripsy pulse.

Author Manuscript Author Manuscript Author Manuscript Author Manuscript

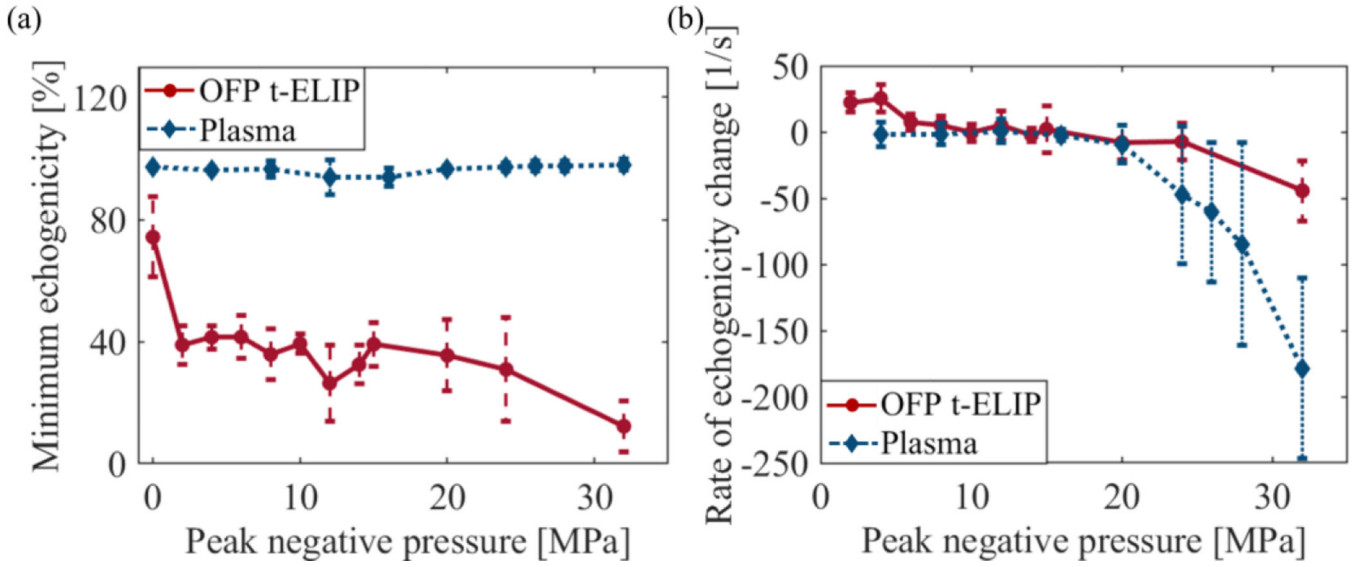

Figure 9.

(a) The minimum echogenicity reflects the reduction in average grayscale intensity within the lumen prior to and after histotripsy exposure. (b) Observed rate of change of grayscale intensity as a function of the pulse pressure.

Author Manuscript
Author Manuscript
Author Manuscript
Author Manuscript

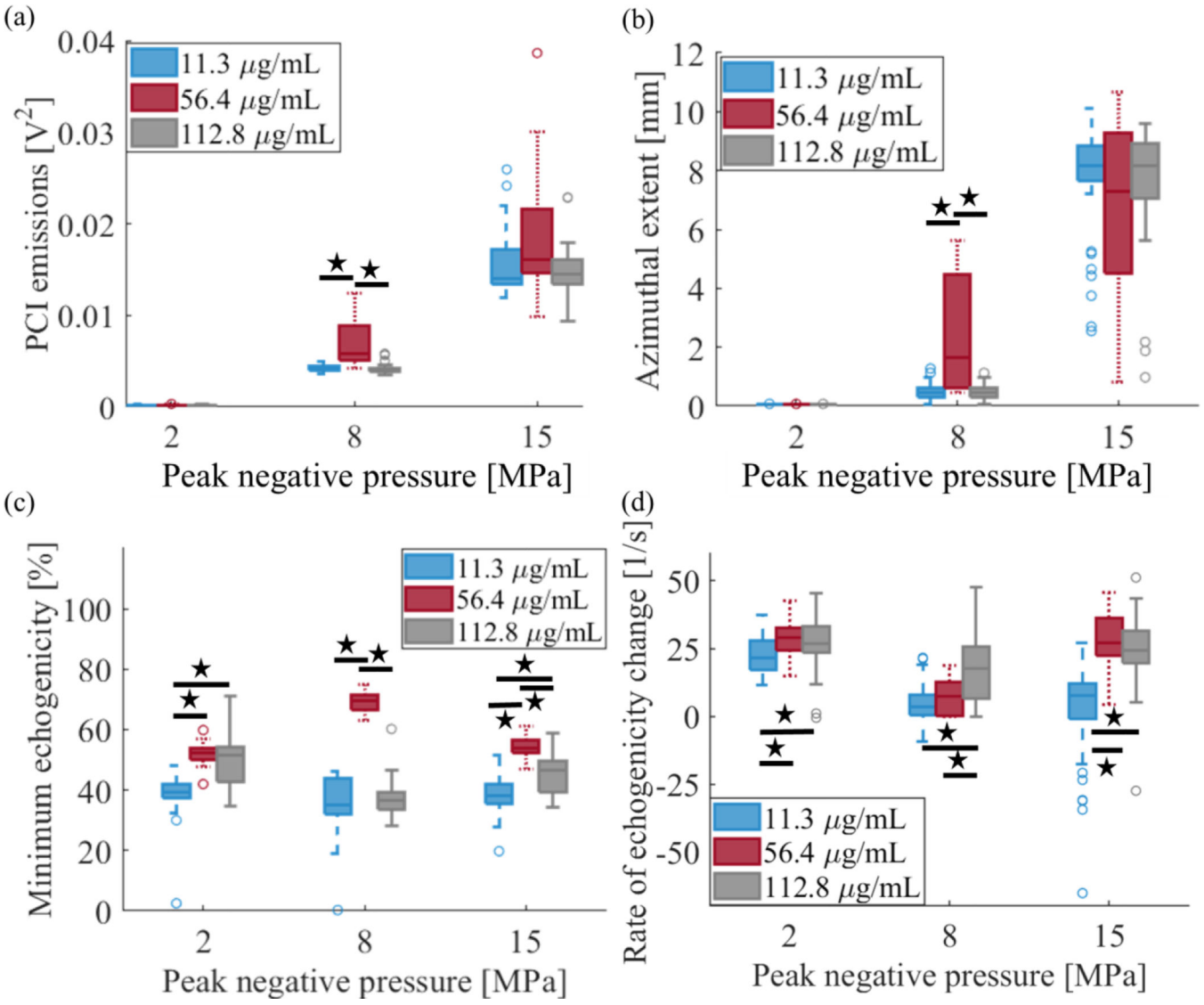

Figure 10.

(a) Maximum acoustic emission levels tracked with passive cavitation imaging, (b) Azimuthal extent of bubble activity based on emissions exceeding that at first threshold (5.7 MPa), (c) Minimum grayscale intensity observed immediately following histotripsy exposure, and (d) Rate of change in grayscale value for different concentrations of OFP t-ELIP.